Materials Advances

ROYAL SOCIETY OF CHEMISTRY

PAPER

View Article Online
View Journal | View Issue

Check for updates

Cite this: *Mater. Adv.*, 2025, **6**, 7067

A comparison of smart window approaches with polymer-modified and gel-glass dispersed liquid crystals

Chung-Hao Chen, [a] Yaiza Lozano Vilches, [b] David Levy[b] and Ingo Dierking *[a]

Received 17th June 2025,
Accepted 27th August 2025

DOI: 10.1039/d5ma00646e

rsc.li/materials-advances

Various approaches to smart windows, including polymer-stabilised, polymer-dispersed, and gel-glass dispersed liquid crystals (GDLC), are discussed with respect to their electro-optic performance based on diffuse reflectivity. The diffuse backward scattering of different devices under an electric field is analysed in detail. The study focuses on the novelty of GDLCs, which utilised a sol–gel derived matrix embedded with a nematic liquid crystal. The unique porous architecture and surface anchoring of GDLCs enhances the electro-optic properties. A comparison between three polymer-modified liquid crystal systems and the GDLC system demonstrates that GDLC provide new opportunities for optical devices, exhibiting lower switch-on voltage, smaller voltages required to achieve stable states and small voltage hysteresis.

Open Access Article. Published on 29 August 2025. Downloaded on 6/12/2026 8:38:17 AM.
This article is licensed under a Creative Commons Attribution-NonCommercial 3.0 Unported Licence.

1. Introduction

Smart windows are innovative electro-optic devices that play a crucial role in intelligent buildings by controlling the transmission of light and heat radiation in response to external stimuli.[1–3] This technology is recognised as a promising approach for improving energy efficiency. Liquid crystal (LC)-based smart windows can dynamically modulate the light transmittance through changes in the orientation of LC molecules.[4–6] In this paper, we discuss the electro-optic, dielectric properties of four LC-based devices: polymer dispersed liquid crystal (PDLC), polymer stabilised liquid (PSLC), polymer stabilised cholesteric texture (PSCT) and gel-glass dispersed liquid crystal (GDLC).

Polymer-modified liquid crystals consist of a polymer matrix filled with liquid crystal material. These composites combine the unique properties of a liquid crystal with the elastic interaction of a large surface and the structural benefits of polymers. In general, polymer-modified liquid crystals can be divided into two categories. The first is known as polymer dispersed liquid crystals (PDLC),[7–13] containing a large proportion of polymer, typically 50% or more. In this system, a continuous polymer matrix incorporates droplets of the liquid crystal phase. PDLCs are usually formed through thermal polymerisation or UV polymerisation of a photoinitiated monomer. UV polymerisation offers several advantages over thermal polymerisation, including easier control of the intensity, dose and duration of polymerisation. Photo-polymerisation can be carried out under controlled temperatures, which is particularly beneficial for liquid crystal systems that may undergo phase changes with temperature variation. During the polymerisation process, phase separation occurs between the liquid crystal and the polymer, transforming the mixture into a continuous polymer embedded with liquid crystal droplets, as shown in Fig. 1(a). The optic axes of the liquid crystal droplets are randomly oriented due to the boundaries of the polymer matrix, resulting in a scattering state at zero applied voltages. At sufficiently large applied electric fields the nematic director within the LC droplets roughly orients along the electric field and the axis of light propagation, (provided positive dielectric anisotropy). If the liquid crystal refractive index along the director is matched to that of the polymer matrix, this will result in a transmissive state.[14,15]

The second category is called polymer stabilised liquid crystals (PSLC),[16–23] sometimes referred to as polymer stabilised cholesteric textures (PSCT)[24–28] when involving cholesteric or chiral nematic liquid crystals. PSLCs are typically formed with a polymer concentration below 10%. In this system, a bifunctional photoreactive monomer, which often is mesogenic by itself, is uniformly dispersed in the liquid crystal. The monomer aligns with the director field of the liquid crystal and after polymerisation, the composite consists of a crossed-linked polymer network with the liquid crystal distributed within it (Fig. 1(b)). The polymer network follows the order of the LC in which it was polymerised, and the device exhibits a bi-continuous structure. Using the Freedericksz effect one would

[a] *Department of Physics and Astronomy, University of Manchester, Oxford Road, Manchester M139PL, UK. E-mail: ingo.dierking@manchester.ac.uk*
[b] *Instituto de Ciencia Materials de Madrid, ICMM. CSIC, Madrid, Spain*

© 2025 The Author(s). Published by the Royal Society of Chemistry

Open Access Article. Published on 29 August 2025. Downloaded on 6/12/2026 8:38:17 AM.
This article is licensed under a Creative Commons Attribution-NonCommercial 3.0 Unported Licence.

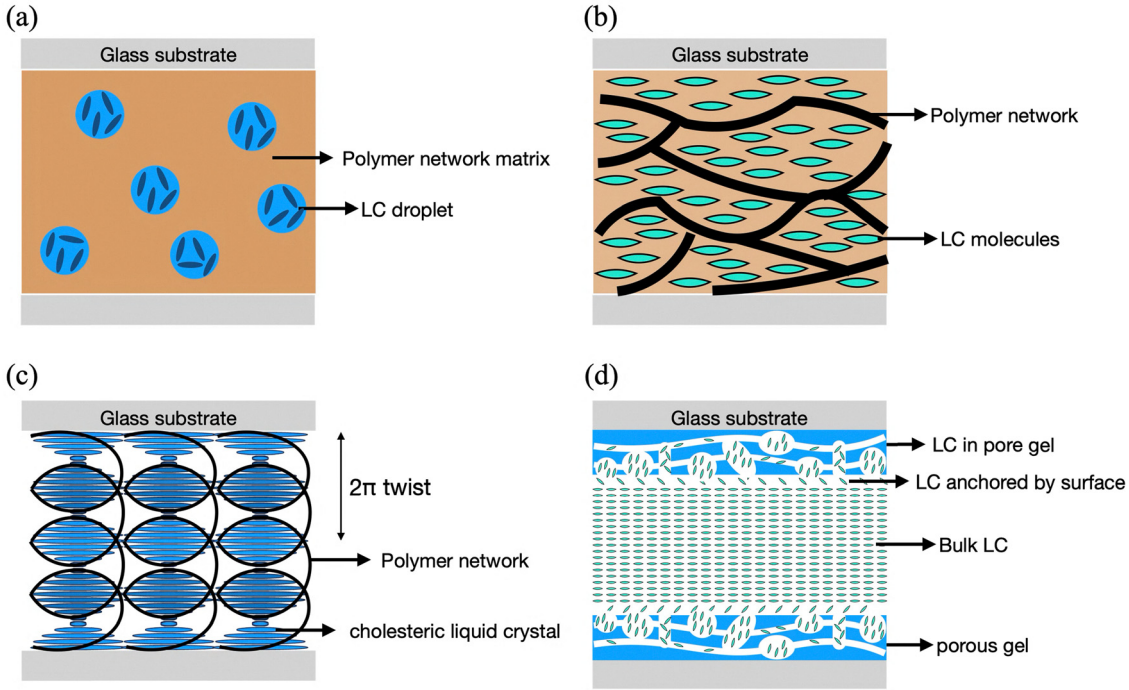

Fig. 1 Schematic illustration of (a) a polymer-dispersed liquid crystal device (PDLC), (b) a polymer-stabilised nematic device (PSLC), (c) a polymer-stabilised cholesteric texture (PSCT), and (d) a gel-glass dispersed liquid crystal (GDLC).

normally drive such a device in the following: at zero electric field maximum transmission of a nematic device can be achieved when orienting the optic axis at 45° between crossed polarisers. Application of an electric field reorients the optic axis parallel to the direction of light propagation, resulting in a non-birefringent, dark state (again assuming positive dielectric anisotropy). Yet here we are interested in scattering properties, so that respective measurements were taken without crossed polarisers applied and changes in intensity are small as compared to those of the Freedericksz effect.

Fig. 1(c) shows a schematic illustration of a polymer-stabilised cholesteric texture. The helical cholesteric order is transferred onto the polymer network, so that a continuous helical polymer network is observed which acts as a template of the liquid crystalline phase during the polymerisation process. In an electro-optic device with a long pitch helical superstructure only a very small reflectivity is observed for zero applied field and the device is transmissive. At applied fields the helical liquid crystal structure deforms and eventually breaks up and a scattering, non-transmissive state is reached.

PDLCs, PSCTs and GDLCs are devices which are based on light scattering and do not rely on crossed polarisers. The scattering results from domains of changing birefringence on spatial scales of the wavelength of light. PSLCs based on nematic liquid crystals on the other hand generally rely on birefringence effects and would be driven between crossed polarisers, while the polymer network stabilises a director orientation. In general, PDLCs and GDLCs do not require polarisers for operation, as their switching relies on electrically controlled light scattering, enable transparency/opacity changes without polarisers. In PSCTs a uniform non-scattering state is electrically switched into a scattering state by breaking up the uniform director field into small domains of varying birefringence. Also, PSCTs are driven without polarisers. The dielectric anisotropy determines the LC reorientation under an applied field, *e.g.* the rise time, or switching on time. Elasticity, which is influenced by the polymer and its morphology, determines the optical response when the electric field is removed, *e.g.* the fall time, or switching off time. The threshold voltage is determined by the anchoring interactions between liquid crystal and polymer structure. Here we study the scattering properties of all these devices, thus their scattering response without use of polarisers, except for response times.

Gel-glass dispersed liquid crystals (GDLCs) rely on the formation and dispersion of liquid crystal microdroplets into a thin gel-glass film.[29–31] The nematic directors of the liquid crystal droplets are randomly oriented due to the anchoring conditions at the droplet–matrix interface, inducing a scattering state at zero applied voltages. When an electric field is applied and the LC has positive dielectric anisotropy, the nematic director tends to align with the direction of light propagation. The refractive index is then matched to that of the matrix, resulting in a transmissive state.[32,33] These materials offer great transparency and enhanced thermal stability due to the inorganic nature of the sol–gel matrix. In this work, a modified GDLC system is studied, where the LC is not confined within disperse droplets but instead is distributed throughout a porous inorganic network (Fig. 1(d)). The electro-optic effect of GDLCs will be discussed below, and its properties are strongly influenced by the interface between the LC and the gel matrix. Optimising

© 2025 The Author(s). Published by the Royal Society of Chemistry

Open Access Article. Published on 29 August 2025. Downloaded on 6/12/2026 8:38:17 AM. This article is licensed under a Creative Commons Attribution-NonCommercial 3.0 Unported Licence.

GDLCs involves reducing the voltage required for switching, minimising switching times and maximising the difference in transmittance between on/off (scattering/non-scattering) states.

We prepared all four of these devices for a comparative investigation of their performance. All devices were prepared under as equal as possible conditions, with equal cell gap, the same liquid crystal used, consistent polymerisation *etc.*, and investigations were performed at equivalent conditions, as far as possible, *e.g.* same equipment, experimental setup, room temperature, applied voltages, and the like. While the response dependence on preparation conditions has been reported in detail for PDLCs, PSLCs and PSCTs, even for different phases (nematic, cholesteric, ferroelectric SmC*), this is not the case for GDLCs. Respective studies are presently being carried out and will be published in due time. Yet, they are not of direct relevance to this comparative investigation.

2. Experimental method and sample preparation

The liquid crystal material employed is the standard room-temperature thermotropic nematic 4-cyano-4′-pentylbiphenyl (5CB) and was selected, because it forms the basis of many commercial mixtures in application devices. It exhibits a phase sequence of Cr 22.5 N 35 I on heating (all temperatures in °C). The PDLC sample was produced *via* photo-polymerisation of a 5CB/NOA60 mixture at 60/40 weight% ratio. The PSLC and PSCT samples were also prepared using photo-polymerisation. The PSLC mixture was composed of 5CB with 4% of mesogenic monomer RM257 (2-Methyl-1,4-phenylene bis (4-(3-(acryloyloxy) propoxy) benzoate), and a very small amount of photo-initiator BME (2 wt% of monomer content). The monomer was directly added to the liquid crystal, and the mixture was sonicated for 15 minutes in an ultrasonic bath under dark conditions. For the PSCT sample, 0.25 wt% of chiral dopant S5011 ((11)-9-(4-propyl-cyclohexyl)-9-10-dihydro-8*H*-dinaphtho [2,1-*f*:1′,2′-*h*][1,5]dioxonine) was incorporated to achieve a helical pitch of approximately 4 μm. The photo-initiator BME (benzoin methyl ether) was dissolved in isopropanol at 5 wt% and added to the LC–monomer mixture at a small amount of 2% of the polymer concentration and then sonicated for 15 minutes. The mixture was placed on a hotplate (IKA C-MAG HP 10) at 40 °C under darkroom conditions until the isopropanol had completely evaporated. The polymer-modified LC mixtures (PDLC, PSLC, PSCT) were filled into a homogeneous cell of gap $d \approx 8$ μm with planar boundary conditions *via* capillary action under darkroom conditions. Finally, the samples were irradiated with UV light (NeoLab UV lamp) at maximum wavelength $\lambda_{max} = 380$ nm and intensity $I_0 = 0.06$ mW cm^{-2}) for 90 min to assure complete polymerisation of the monomers.

The preparation of the GDLC sample involved two main steps. First, the sol–gel porous coatings were prepared using an oil-templated sol–gel method. The initial sol–gel solution was prepared by mixing the silica precursor TMOS (tetramethyl orthosilicate) with ethanol, water and hydroxyacetone, which acted as the catalyst. This solution was then left to react for one day at 40 °C, after which a certain amount of castor oil (1.5% w/v) was added prior to deposition. A small volume (200 μL) of the solution was deposited by spin coating at 1800 rpm onto transparent ITO-coated conductive glasses to form the thin films ($\approx$0.3μm). The samples were then dried in an oven at 80 °C for 2 h and thoroughly rinsed with ethanol and acetone to remove the oil and access to the intrinsic porosity of the films. The second step involved assembling two sol–gel coated substrates into a sandwich cell ($\approx$8 μm) using adhesive tape to fix the substrates. The sol–gel cells were filled with 5CB through capillary action from the edges. The cells were slightly heated prior to capillary action to enhance 5CB infiltration into the porous network.

The electro-optical properties that were measured included threshold voltage, backward scattering/diffuse reflectivity and response time. Scattering was measured for increasing as well as decreasing applied voltages to be able to determine the possibility of hysteretic behaviour and quantify hysteresis. The measurements were also used to determine the contrast ratio of the various devices.

Electro-optic properties were investigated through scattering studies performed with an integrating sphere. The experimental setup is shown in Fig. 2. The modular multi-port integrating sphere (Thorlabs, 4P4) provides a durable, highly reflective surface to diffuse light. A HeNe laser (Thorlabs, HNL020LB) serves as the incident light source. A photodiode (Thorlabs, SM05PD2A) connected with the integration sphere and a voltage metre (Agilent, 34401A) measure the scattered light intensity. The voltage with frequency $f = 1$ kHz applied to the sample cells was generate by an LCR meter (Agilent E4980A). When the laser light falls onto the sample device, the primary transmitted and reflected light exits the integrating sphere without detection, while the diffusely reflected scattered light is detected by the photodiode.

The threshold voltage of the devices was determined by capacitance measurements using the LCR meter (Agilent E4980A). A sine AC voltage of frequency $f = 1$ kHz was applied to the device at slowly increasing amplitude and the capacitance determined as a function of voltage in parallel equivalent circuit mode. As the liquid crystal director begins to reorient, the capacitance changes, indicating the threshold voltage. Since capacitances can be determined with high precision, this method is preferable over optic measurements of the threshold.

3. Results and discussion

Polarising optical microscopy (POM) textures of the different devices are shown in Fig. 3. The PDLC displays the expected droplet morphology, where LC droplets are dispersed in a polymer matrix, forming birefringence domains under cross-polarisers (Fig. 3(a)). In PSLC system, the web-like polymer network stabilises the liquid crystal, producing a dark state position when the LC director aligns parallel to the polariser (Fig. 3(b)). The PSCT exhibits a helical structure characteristic

Open Access Article. Published on 29 August 2025. Downloaded on 6/12/2026 8:38:17 AM.
This article is licensed under a Creative Commons Attribution-NonCommercial 3.0 Unported Licence.

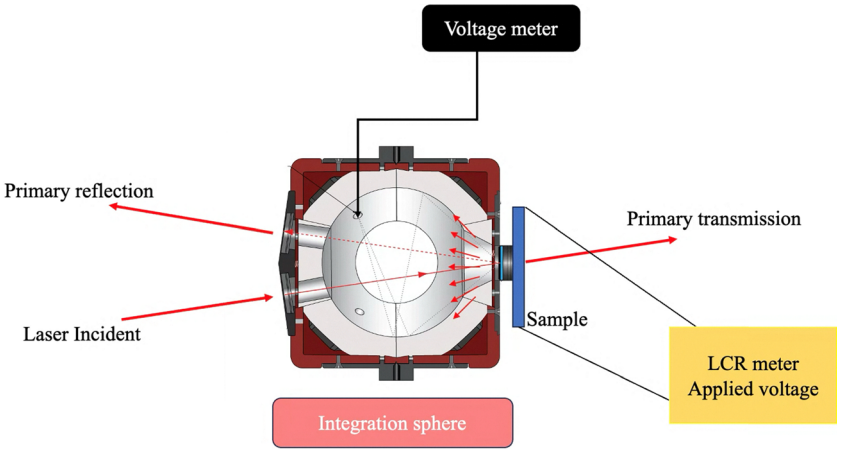

Fig. 2 Schematic illustration of the use of an integrating sphere to determine the laser backward scattering, *i.e.* diffuse reflectivity of a device.

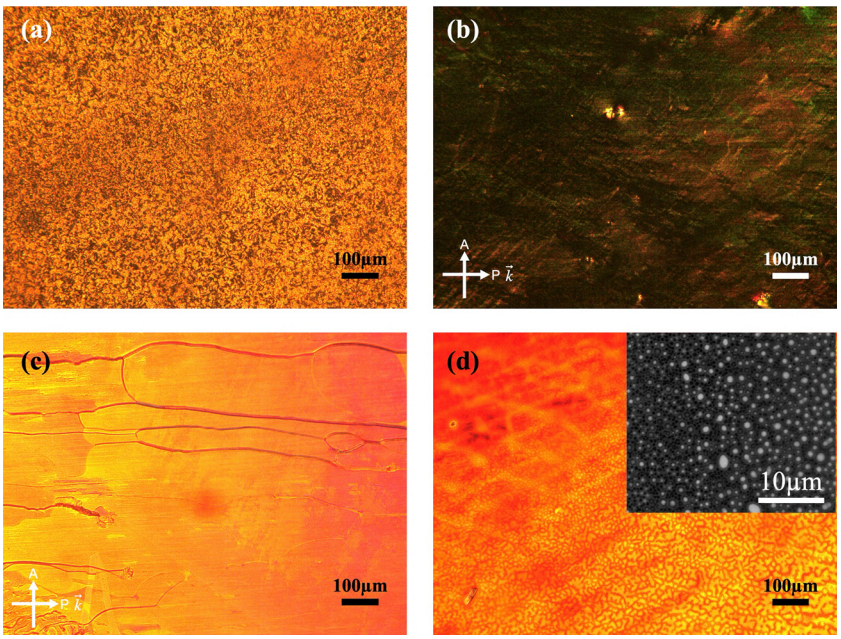

Fig. 3 Polarising optical microscopy images of (a) the PDLC, (b) the PSLC, (c) the PSCT and (d) the GDLC, where the inset shows the SEM image of the device at a smaller scale than optical microscopy.

of the chiral nematic phase, with visible oily streaks (Fig. 3(c)), while the GDLC adopts a basically planar alignment at room temperature (Fig. 3(d)).

The first set of results comparing the performance of PDLCs, PSLCs, PSCTs and GDLCs is focused on the static properties derived from the diffuse back-scattering under applied voltage. This was measured with a geometry according to Fig. 2 and by gradually increasing the voltage to roughly 10 V and then decreasing it back to 0 V. For these measurements care had to be taken to avoid dielectric breakdown at larger voltages. Fig. 4 summarises the laser backward scattering data obtained after first heating into isotropic phase to erase the thermal history before starting the electric field application at room temperature.

As expected, the PDLC exhibited the scattering state initially with the scattering intensity decreasing as the applied voltage is increased and the liquid crystal contained in the droplets slowly orienting along the electric field direction, reaching the position of index matching. The back-scattered intensity will then stay constant, with the low value indicating the unavoidable scattering due to substrates and polymer matrix (Fig. 4(a)).

For the PSLC, the scattering remained stable and low up to 6 V, after which it increased with further increases in voltage. This indicates an increased threshold voltage as compared to the neat liquid crystal 5CB ($V_{th} \sim 0.7$ V), which is due to the much-increased elastic interactions between liquid crystal and the largely enhanced surface area due to the dispersed polymer network for the polymer stabilised system. The increased scattering is caused by an increasing mismatch between the refractive indices of the polymer and the liquid crystal for increasing voltage (Fig. 4(b)).

© 2025 The Author(s). Published by the Royal Society of Chemistry

Open Access Article. Published on 29 August 2025. Downloaded on 6/12/2026 8:38:17 AM.
This article is licensed under a Creative Commons Attribution-NonCommercial 3.0 Unported Licence.

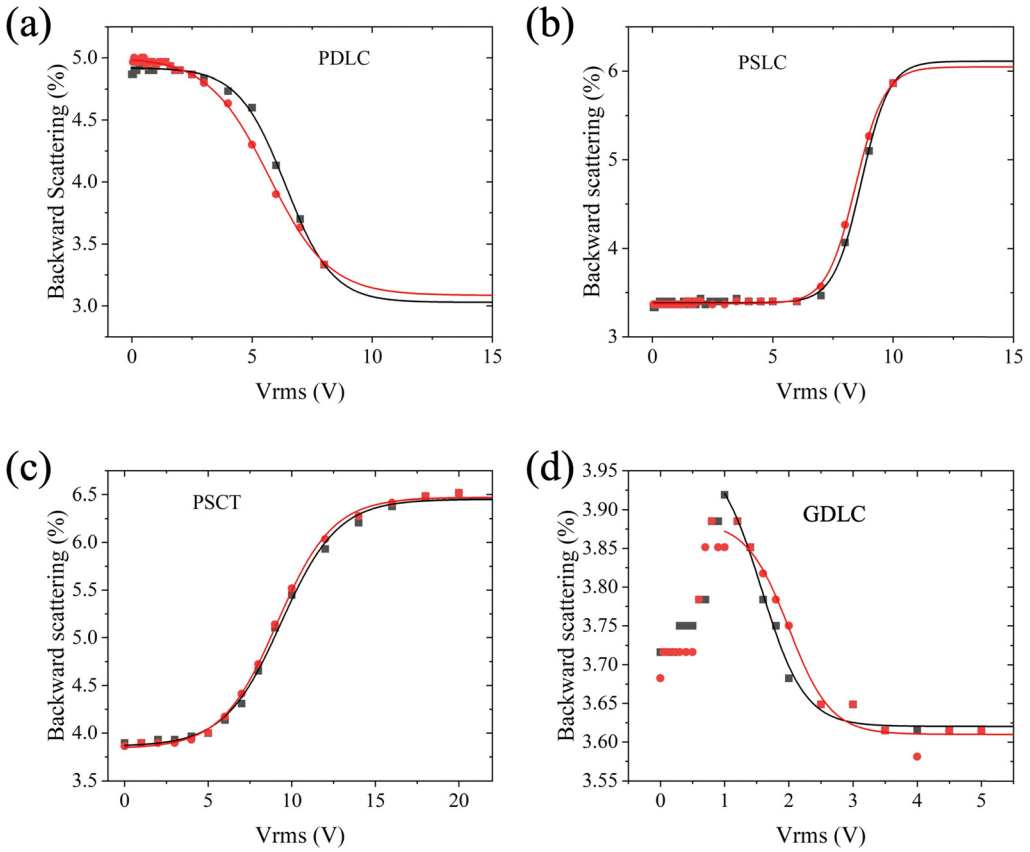

Fig. 4 Backward laser scattering measurements for (a) PDLC, (b) PSLC, (c) PSCT and (d) GDLC under an applied field. Data were recorded during voltage increase (black symbols) and decrease (red symbols).

PSCTs exhibit a similar scattering behaviour, maintaining a low back-scattering due to substrates and polymer network, until at about 4 V the threshold for reorientation and breaking up of the helical superstructure is reached and the back scattering rises rapidly for increasing voltage (Fig. 4(c)).

The GDLC device exhibited a scattering behaviour which is slightly more complex and can be understood as a superposition of PSLC and PDLC for low and higher voltages, respectively. The initial zero-volt state exhibits a low scattering intensity which is again due to glass substrates and possibly thin sol–gel areas at the interface. At low threshold voltage, comparable to the neat LC, the bulk liquid crystal begins to reorient, resulting in increased scattering due to refractive index mismatch at the interface to the porous gel structure. Beyond 1 V, the scattering decreases and the transparency increases for increasing voltage, as homeotropic alignment in the bulk LC is achieved and the contribution from LC trapped inside the pores is further reduced due to improved alignment along the applied electric field direction (Fig. 3(d)). The higher scattering in the low-field state is thus caused by surface anchoring between the LC molecules and the porous-gel structure. Therefore, the dominant contribution to the electro-optic response arises from the bulk LC at the interface, which undergoes significant reorientation under the applied field. The influence of LC confined within the porous network appears to be comparatively minor, likely due to limited infiltration or small pore volume.

For applications such as privacy windows or smart glass, the hysteresis should be minimal to ensure the equivalent performance during voltage increase/decrease, both when switching the device on and off. The scattering hysteresis can be estimated from the backscattering curves going up and down in voltage, as demonstrated in Fig. 5(a) for the GDLC device. The curves for increasing (black) and decreasing (red) voltages can be approximated by sigmoidal curves. The maximum hysteresis can then be read off as the voltage difference at the 50% level between the highest and the lowest scattering values. Applying this procedure to all different devices, leads to the comparative bar chart depicted in Fig. 5(b).

Voltage saturation can be defined as the applied voltage required to achieve stabile scattering. The polymer-modified liquid crystals begin to exhibit scattering changes at approximately 5 V, with saturation occurring between 5 to 10 V, while the GDLC displayed the highest scattering at 1 V, after which scattering decreased with increasing voltage. Saturation for GDLC occurred at 3.5 V, corresponding to a saturation range of 2.5 V (1–3.5 V). The GDLC exhibits a significantly lower voltage saturation compared to polymer-modified liquid crystals, indicating it requires much lower operating voltages. These results are consistent with backward laser scattering

Open Access Article. Published on 29 August 2025. Downloaded on 6/12/2026 8:38:17 AM.
This article is licensed under a Creative Commons Attribution-NonCommercial 3.0 Unported Licence.

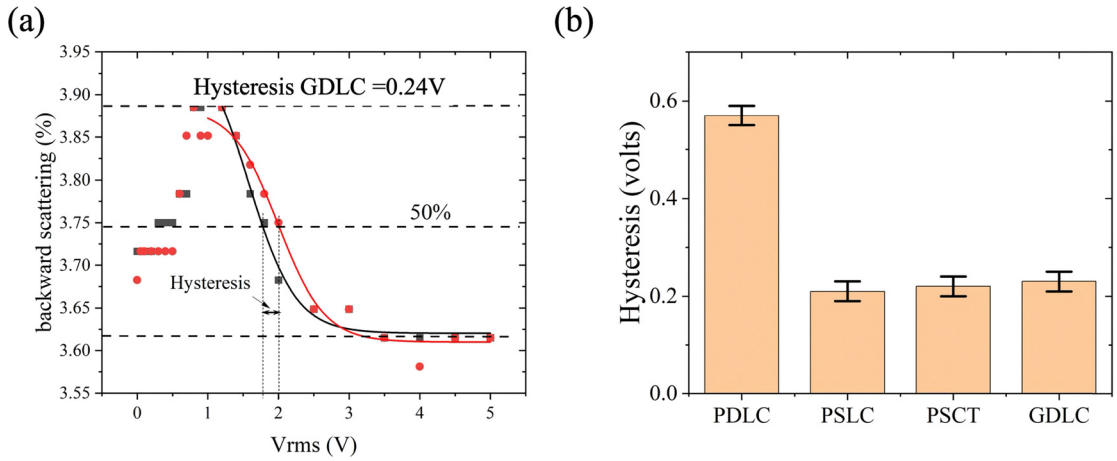

Fig. 5 (a) Schematic illustration on how the hysteresis was determined, presented for the GDLC sample. (b) Comparison of determined hysteresis values for all four types of devices.

measurements, that confirm the greater influence of the bulk LC on the overall scattering and electro-optic properties.

The hysteresis analysis indicates that the PDLC device exhibits the largest hysteresis, while the polymer-stabilised and the gel-glass devices exhibit a comparable but clearly smaller hysteresis. This can be attributed to the fact that the surface anchoring within a confined LC droplet within a PDLC is considerable stronger than the more porous structure of a PSLC, PSCT or GDLC, which all contain at least some fraction of bulk-like, non-interface dominated liquid crystal. PSLC, PSCT and GDLC exhibit approximately the same void size distribution. This is reflected by the very similar and small hysteresis observed for all three devices, resulting from a continuous network being dispersed in a continuous liquid crystal phase, *e.g.* sponge-like structures (Fig. 1(b)–(d)). In contrast, the PDLC consists of encapsulated LC droplets within a continuous polymer matrix, which results in larger anchoring energy, and greater hysteresis. In GDLC samples, the liquid crystal molecules can roughly be placed into three categories: (i) those inside the gel pores, (ii) those in contact with the gel surface and (iii) bulk molecules between the two substrates. The lower hysteresis in the GDLC device suggests that the electro-optic response is dominated by the bulk LC molecules between the two substrates.

As mentioned above, threshold measurements were carried out by determination of the capacitance of device cells. Fig. 6(a) illustrates the calculation of the threshold voltage by fitting a straight line to the low voltage regime of the data where the capacitance is constant, and another to the regime of the largest changes of capacitance. The crossing point of both lines provides a reproducible and comparative measure for the threshold voltage to within 0.05 V. The comparison of the threshold voltages for the four different devices is shown in Fig. 6(b). To recall from literature, the threshold voltage of neat 5CB is approximately 0.7 to 0.8 V[34–37] which is well reproduced in our study for a planar cell. For PDLCs, PSLCs and PSCTs, we observe a comparable value for the threshold voltage of around 5 V. The GDLC, however, shows a significantly lower threshold voltage. This is because a large proportion of LC molecules are free and bulk-like between the two gel-pore substrates. From the threshold voltage measurements, it is clear that the surface anchoring of the LC on the thin gel film/layer is much lower than that caused by the polymer confinement. As a result, the GDLC exhibits a threshold comparable to that of neat 5CB.

We can now focus on the dynamic properties of the different device cells and related quantities which are of importance for applications. Response times were measured by analysing light

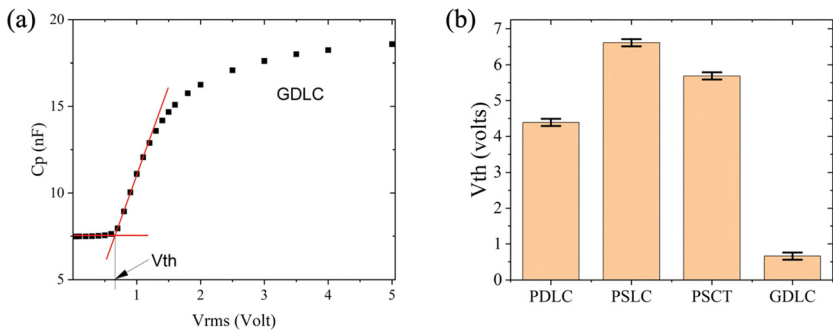

Fig. 6 (a) Schematic illustration of the determination of the threshold voltage using data obtained from the GDLC device. (b) Bar chart comparing the threshold voltage, V_{th}, for the four different devices.

© 2025 The Author(s). Published by the Royal Society of Chemistry

Open Access Article. Published on 29 August 2025. Downloaded on 6/12/2026 8:38:17 AM.
This article is licensed under a Creative Commons Attribution-NonCommercial 3.0 Unported Licence.

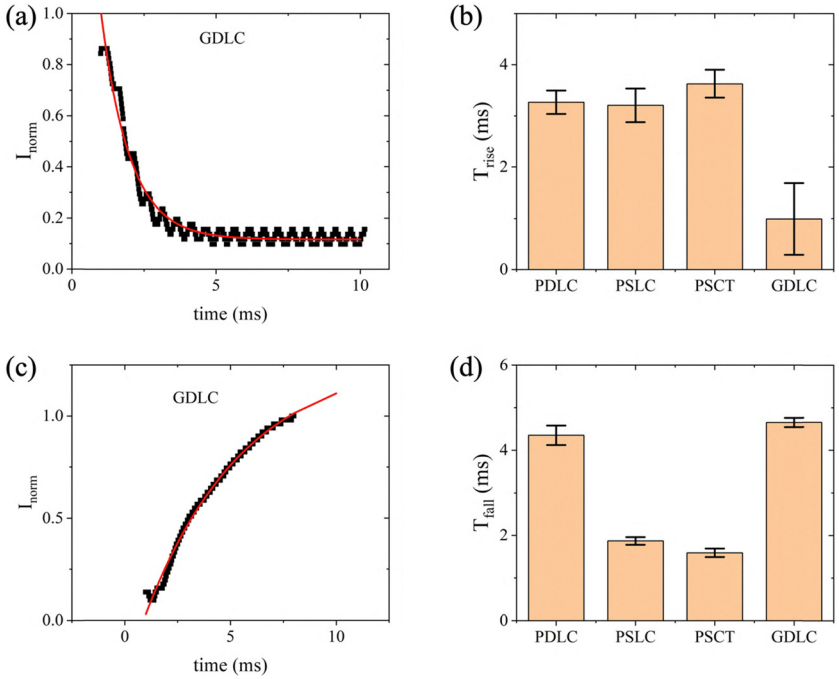

Fig. 7 Response time analysis: (a) response raise time calculated from transmission measurements using GDLC as an example. (b) Bar chart comparing τ_{rise} value across four materials. (c) Response fall time calculated from transmission measurements using GDLC as an example. (d) Bar chart comparing τ_{fall} value across the four different devices.

transmission changes after applying a 13.7 Hz square wave modulated by a sine AC 5V voltage with frequency f = 1 kHz. The transmission curves were fitted using an exponential decay function $e^{\left(-\frac{t}{\tau}\right)}$, where τ_{rise} represents the rise time and τ_{fall} the fall time. The results are depicted in Fig. 7.

The polymer modified liquid crystals exhibit a longer rise time. The rise time for the PDLC is 3.3 ms. In the PDLC, the LC droplets are confined by the polymer matrix, which restricts their movement. Compared to the bulk liquid crystal, the confinement prolongs the reorientation process on field application due to strong surface anchoring. Similarly, the polymer networks introduce additional surface anchoring and elastic forces. The LC director must overcome greater resistance to reorientation, resulting also in a longer rise time when switching on. The response rise time for PSLC and PSCT are 3.2 ms and 3.6 ms, respectively. In contrast, the GDLC exhibits a much quicker rise time of 1 ms, due to the weaker surface anchoring, which allows the LC molecules to reorient more easily. Additionally, a large proportion of LC molecules remain bulk-like, free between the two gel-pore substrates, further reducing anchoring and thus response time τ_{rise}.

On the contrary, PSLC and PSCT exhibit quicker switch off (relaxation) times τ_{fall} of 1.9 ms and 1.6 ms, respectively, due to the elastic restoring force from the polymer network. The horizontally oriented polymer strands and cross-linked network act as a template, favouring the original position of the LC molecules during polymerisation. When the applied field is removed, the network drives the LC back to the initial orientation, resulting in a fast switching off process.

In contrast, PDLC and GDLC exhibit longer relaxation times of 4.4 ms and 4.7 ms, respectively, as both lack strong elastic restoring forces. In the case of PDLC, this is due to isolated droplet confinement, while for GDLC, it is due to the dominance of unconfined bulk-like LC with minimal structural memory.

It should be noted that none of these devices are conceptually made with fast switching on mind. The total response times (τ_{rise} + τ_{fall}) are of the order of 6–7 ms for all devices, which is of sufficient speed for privacy windows and smart glass, the main applications of these materials.

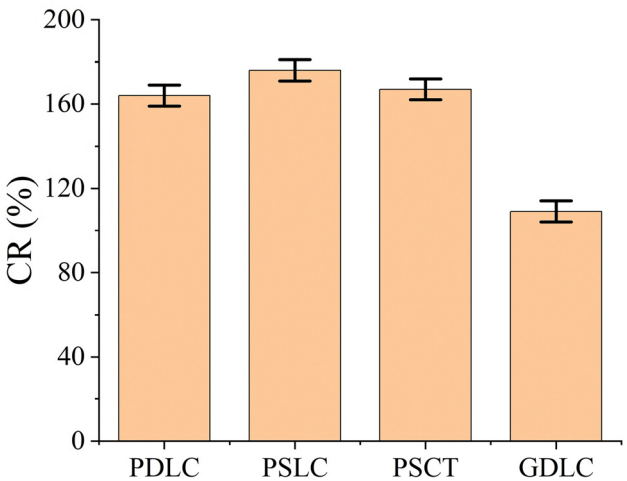

Fig. 8 Contrast ratio comparing of the four smart glass device structures.

Open Access Article. Published on 29 August 2025. Downloaded on 6/12/2026 8:38:17 AM. This article is licensed under a Creative Commons Attribution-NonCommercial 3.0 Unported Licence.

The contrast ratio of the four devices was also analysed (Fig. 8). It is calculated as the ratio of maximum (off state) to minimum scattering intensity (on state). Among the four devices, the GDLCs shows a somewhat lower contrast ratio; nevertheless, it requires significantly smaller voltage to reach saturation. The scattering region of the GDLC is the interface layer between the substrate and the uniform LC, thus the porous gel layer with its interface to the liquid crystal. The thickness of this layer is considerably thinner (2–3 μm in total), compare to the 8 μm cell gap in other devices, where the entire layer contributes to scattering, resulting in a higher contrast ratio. The contrast ratios for the diffuse back scattering of the polymer modified liquid crystals are around 1.6, indicating that these devices can achieve better performance in term of contrast ratio, but they require a much higher voltage to switch on, thus also higher energy consumption (Fig. 8).

4. Conclusions

To summarise, PSLCs and PSCTs exhibit the smallest voltage hysteresis, followed by GDLCs, while PDLCs shows the greatest voltage hysteresis among the four device types. Overall, the GDLC represents a novel electro-optic device with a lower threshold voltage, smaller contrast ratio, shorter switch on and longer switch off response time, and a significantly smaller voltage saturation range. This design enables energy-efficient performance and excels in low-voltage smart windows requiring decent contrast. Conversely, PSLCs are better suited for dynamic applications and high-speed optical devices. In general, the performance of different types of smart glass devices is always a trade-off between reflectivity and speed *versus* low energy consumption and low voltage. As such, GDLCs can be seen as a clearly rising competitor to the standard PDLCs.

Conflicts of interest

There are no conflicts to declare.

Data availability

The data supporting this article have been included in the publication and as part of the SI. See DOI: **https://doi.org/10.1039/d5ma00646e**

References

1 Y. Ke, *et al.*, Smart windows: electro-, thermo-, mechano-, photochromics, and beyond, *Adv. Energy Mater.*, 2019, **9**(39), 1902066.
2 S. Wu, *et al.*, Applications of thermochromic and electrochromic smart windows: Materials to buildings, *Cell Reports Phys. Sci.*, 2023, **4**, 5.
3 L. Long and H. Ye, How to be smart and energy efficient: A general discussion on thermochromic windows, *Sci. Rep.*, 2014, **4**(1), 6427.
4 E. Castellón and D. Levy, Smart windows based on liquid crystal dispersions, *Transparent Conduct. Mater.*, 2018, 337–365.
5 W. Shen and G. Li, Recent progress in liquid crystal-based smart windows: materials, structures, and design, *Laser Photon. Rev.*, 2023, **17**(1), 2200207.
6 R. Baetens, B. P. Jelle and A. Gustavsen, Properties, requirements and possibilities of smart windows for dynamic daylight and solar energy control in buildings: A state-of-the-art review, *Solar Energy Mater. Solar Cells*, 2010, **94**(2), 87–105.
7 L. Bouteiller and P. L. Barny, Polymer-dispersed liquid crystals: preparation, operation and application, *Liq. Cryst.*, 1996, **21**(2), 157–174.
8 S. Agarwal, *et al.*, A Comprehensive Review on Polymer-Dispersed Liquid Crystals: Mechanisms, *ACS Mater. Au*, 2024, **5**(1), 88–114.
9 S. Bronnikov, S. Kostromin and V. Zuev, Polymer-dispersed liquid crystals: progress in preparation, investigation, and application, *J. Macromol. Sci., Part B: Phys.*, 2013, **52**(12), 1718–1735.
10 N. Nasir, *et al.*, Polymer-dispersed liquid-crystal-based switchable glazing fabricated via vacuum glass coupling, *RSC Adv.*, 2020, **10**(53), 32225–32231.
11 A. Rešetič, *et al.*, Polymer-dispersed liquid crystal elastomers, *Nat. Commun.*, 2016, **7**(1), 13140.
12 D. Cupelli, *et al.*, Self-adjusting smart windows based on polymer-dispersed liquid crystals, *Solar Energy Mater. Solar Cells*, 2009, **93**(11), 2008–2012.
13 J. W. Doane, *Polymer dispersed liquid crystal displays, in Liquid Crystals—Applications And Uses*, 1990, World Scientific, Vol. 1, pp. 361–395.
14 Z. Huang, G. Chidichimo and A. Golemme, The electric field in polymer dispersed liquid crystal droplets and its influence on molecular orientation. Molecular Crystals and Liquid Crystals Science and Technology. Section A, *Mol. Cryst. Liq. Cryst.*, 1998, **312**(1), 165–178.
15 W. Korner, *et al.*, PDLC films for control of light transmission, *J. Phys. D: Appl. Phys.*, 1994, **27**(10), 2145.
16 I. Dierking, Polymer network–stabilized liquid crystals, *Adv. Mater.*, 2000, **12**(3), 167–181.
17 Y. Ye, L. Guo and T. Zhong, A review of developments in polymer stabilized liquid crystals, *Polymers*, 2023, **15**(13), 2962.
18 C. Mahyaoui, *et al.*, Influence of polymerisation parameters on the electro-optical properties of polymer-stabilised liquid crystals for smart glass application, *Liq. Cryst.*, 2024, **51**(12), 1995–2010.
19 H. Kikuchi, *et al.*, Polymer-stabilized liquid crystal blue phases, *Nat. Mater.*, 2002, **1**(1), 64–68.
20 A. Bobrovsky, *et al.*, Fast photo-and electro-optical switching of the polymer-stabilised cholesteric liquid crystal composite prepared by the template method, *Liq. Cryst.*, 2023, **50**(7–10), 1563–1572.
21 H. Khandelwal, *et al.*, Electrically switchable polymer stabilised broadband infrared reflectors and their potential as smart windows for energy saving in buildings, *Sci. Rep.*, 2015, **5**(1), 11773.

© 2025 The Author(s). Published by the Royal Society of Chemistry

Open Access Article. Published on 29 August 2025. Downloaded on 6/12/2026 8:38:17 AM.
This article is licensed under a Creative Commons Attribution-NonCommercial 3.0 Unported Licence.

22 S.-M. Guo, *et al.*, Preparation of a thermally light-transmittance-controllable film from a coexistent system of polymer-dispersed and polymer-stabilized liquid crystals, *ACS Appl. Mater. Interfaces*, 2017, **9**(3), 2942–2947.
23 Y. Zhou, *et al.*, Effect of polymer network topology on the electro-optical performance of polymer stabilized liquid crystal (PSLC) devices, *Macromol. Chem. Phys.*, 2020, **221**(18), 2000185.
24 Y. Liu, *et al.*, Broadband reflective bilayer polymer-stabilised cholesteric liquid crystal films capable of shielding visible and near-infrared laser light, *Liq. Cryst.*, 2025, 1–11.
25 T. J. White, *et al.*, Polymer stabilization of phototunable cholesteric liquid crystals, *Soft Matter*, 2009, **5**(19), 3623–3628.
26 M. Mitov, E. Nouvet and N. Dessaud, Polymer-stabilized cholesteric liquid crystals as switchable photonic broad bandgaps, *Eur. Phys. J. E*, 2004, **15**, 413–419.
27 K. M. Lee, *et al.*, Recent advances in electro-optic response of polymer-stabilized cholesteric liquid crystals, *Materials*, 2023, **16**(6), 2248.
28 M. Mitov, Cholesteric liquid crystals with a broad light reflection band, *Adv. Mater.*, 2012, **24**(47), 6260–6276.
29 M. Zayat and D. Levy, The performance of hybrid organic–active-inorganic GDLC electrooptical devices, *J. Mater. Chem.*, 2005, **15**(35–36), 3769–3775.
30 D. Levy, Glass Dispersed Liquid Crystals, *Liq. Cryst. Today*, 1995, **5**(4), 1–2.
31 D. Levy, Sol-Gel materials for optical and electrooptical applications. Sol-Gel Derived Optical and Photonic, *Materials*, 2020, 293.
32 M. Zayat and D. Levy, Surface Organic Modifications and the Performance of Sol−Gel Derived Gel−Glass Dispersed Liquid Crystals (GDLCs), *Chem. Mater.*, 2003, **15**(11), 2122–2128.
33 E. Castellón, M. Zayat and D. Levy, A chemical approach to control the refractive index of sol–gel matrices for liquid-crystal dispersion devices, *J. Sol-Gel Sci. Technol.*, 2016, **78**, 411–421.
34 R. Basu, Effect of carbon nanotubes on the field-induced nematic switching, *Appl. Phys. Lett.*, 2013, **103**, 24.
35 J. W. Goodby, 4′-pentyl-4-cyanobiphenyl-5CB, *Liq. Cryst.*, 2024, **51**(8–9), 1272–1295.
36 M. Mrukiewicz, *et al.*, Threshold voltage decrease in a thermotropic nematic liquid crystal doped with graphene oxide flakes, *Beilstein J. Nanotechnol.*, 2019, **10**(1), 71–78.
37 S. Ghosh, E. Abraham and I. I. Smalyukh, Low-voltage haze tuning with cellulose-network liquid crystal gels, *ACS Nano*, 2023, **17**(20), 19767–19778.